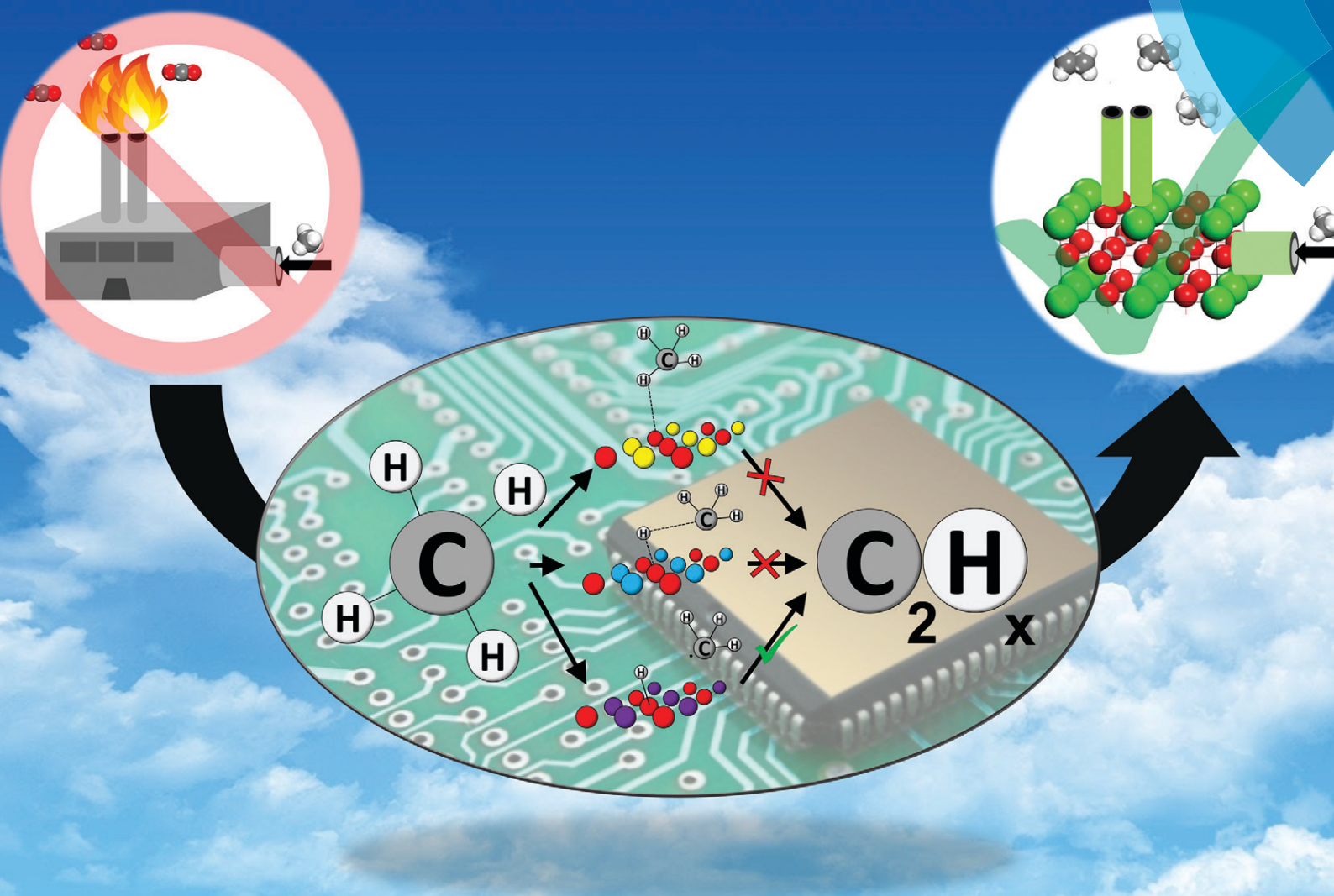


Catalysis Science & Technology

rsc.li/catalysis



ISSN 2044-4761



PAPER

De-en Jiang *et al.*

Exploring perovskites for methane activation from first principles

Cite this: *Catal. Sci. Technol.*, 2018,
8, 702

Exploring perovskites for methane activation from first principles

Victor Fung,^a Felipe Polo-Garzon,^b Zili Wu^b and De-en Jiang *^a

The diversity of perovskites offers many opportunities for catalysis, but an overall trend has been elusive. Using density functional theory, we studied a large set of perovskites in the ABO_3 formula *via* descriptors of oxygen reactivity such as vacancy formation energy, hydrogen adsorption energy, and the first C–H activation energy of methane. It was found that changing the identity of B within a period increases the oxygen reactivity from the early to late transition metals, while changing A within a group has a much smaller effect on oxygen reactivity. Within the same group, B in the 3d period has the most reactive lattice oxygen compared to the 4d or 5d period. Some perovskites display large differences in reactivity for different terminations. Further examination of the second C–H bond breaking on these perovskites revealed that larger A cations and non-transition metal B cations have higher activation energies, which is conducive to the formation of coupling products instead of oxidation to CO or CO_2 . Balance between the first C–H bond breaking and methyl desorption suggests a just right oxygen reactivity as described by the hydrogen adsorption energy. These insights may help in designing better perovskite catalysts for methane activation.

Received 31st August 2017,
Accepted 24th November 2017

DOI: 10.1039/c7cy01791j

rsc.li/catalysis

1. Introduction

Perovskites are a prominent class of mixed-metal oxides with a wide range of possible compositions and corresponding physical and chemical properties. Following the general formula ABO_3 , the 12-fold coordinated A and 6-fold coordinated B metal cations can be sourced from the majority of the metallic elements in the periodic table, so long as the ionic radii of the constituting elements are suitable for the formation of a cubic perovskite structure, which can be estimated by calculating the Goldschmidt tolerance factor.¹ Deviations from the ideal structural tolerance factor of one may lead to distorted lattices with orthorhombic and rhombohedral structures. As a further level of compositional diversity, the A and B cations can be substituted with additional elements, leading to non-stoichiometric perovskites with cationic or anionic deficiencies. From this wide diversity of possible configurations, a significant portion has been found to have good thermal stability and promising catalytic activity for a wide range of industrially important reactions.^{2–8} It is highly desirable to predict many important catalytic properties of a perovskite from first principles.^{9,10}

Perovskites are extensively studied in photocatalysis and can also be a potential replacement for expensive noble metals for heterogeneous catalysis and electrocatalysis.^{2–6,11,12} Hydrogen adsorption and vacancy formation energies have been shown to be viable ‘descriptors’ of catalytic activity.^{10,13–19} Experimentally, catalysts with high oxygen mobility and low vacancy formation energies are often reactive for a wide range of reactions, because the lattice oxygen often plays a critical role in the catalysis reaction *via* the Mars–van Krevelen mechanism. Similarly, hydrogen adsorption energy is important since it can be linked to the energy barrier of C–H activation *via* a homolytic mechanism. Being able to estimate the energy barrier for C–H activation and relate it to experimental rates is crucial for elucidating favored reaction pathways on metal oxides.²⁰

CH_4 utilization has received renewed interest in recent years due to the increase in shale gas production. Perovskite catalysts have shown excellent thermal stability (up to 1000 °C), resistance to sintering of substituted metals and high oxygen mobility, which offers great potential for methane combustion and oxidative coupling reactions.^{3,5,21–24} These routes for the conversion of methane^{21,25–28} to methanol or ethylene have wide ranging implications for the fuel and chemical industry. For the catalytic reaction of hydrocarbons on metal oxides, C–H bond activation is generally the first step in the reaction.^{13,26,29,30} Following C–H activation, methyl and hydroxyl groups form on the surface lattice oxygens. The

^a Department of Chemistry, University of California, Riverside, California 92521, USA. E-mail: djiang@ucr.edu; Tel: +1 951 827 4430

^b Chemical Sciences Division and Center for Nanophase Materials Sciences, Oak Ridge National Laboratory, Oak Ridge, Tennessee 37831, USA

methyl groups can couple on the surface or in the gas phase to form C₂ products, or can further oxidize to form combustion products such as CO and CO₂.

For perovskites, the (001) surface facet is the stable and experimentally observed^{31–34} facet, though other orientations can exist in high-surface-area or mesoporous structures. To isolate the effect of compositional changes on catalytic activity, this study will focus on the most commonly exposed (001) surface facet. Two possible terminations exist for this facet: the ‘A’ surface with the AO layer at the termination and the ‘B’ surface with the BO₂ layer. Experimentally, it is possible to control the surface termination through various treatments, which has been demonstrated to lead to different catalytic activities and selectivities for reactions.³⁴

The present work aims to understand the catalytic activity of perovskites for methane activation. Taking advantage of the well-defined structure of cubic perovskites and the diversity of possible compositions, we screen a large set of promising perovskites for low C–H activation energies. We first demonstrate the validity of correlating the H-adsorption-energy (HAE) and vacancy-formation-energy (VFE) descriptors with C–H activation energies, and then use these to identify the most plausible active perovskites. Finally, we study whether or not it would be possible to select perovskites that favor C–C coupling and disfavor the further oxidation on the surface.

2. Methods

Density functional theory calculations were performed with the Vienna *ab initio* Simulation Package (VASP).^{35,36} The Perdew–Burke–Ernzerhof (PBE)³⁷ form of the generalized-gradient approximation (GGA) was used for electron exchange and correlation energies. All calculations were performed with spin polarization. The projector-augmented wave method was used to describe the electron–core interaction,^{35,38} and the kinetic energy cutoff was set to 450 eV. For the studied surface slabs, 3 × 3 × 1 sampling of the Brillouin zone with the Monkhorst–Pack scheme was used.³⁹ The D3 correction method by Grimme *et al.* was applied for the van der Waals energy.⁴⁰ The surface slabs of the studied ABO₃ perovskites have three AO layers and three BO₂ layers, with a 15 Å vacuum layer. A 2 × 2 supercell of the lateral unit cell was used in subsequent calculations. The top two layers of the slabs were allowed to relax in all calculations. The vacancy formation energy (E_{vac}) was calculated with the equation

$$E_{\text{vac}} = E_{\text{defect-surface}} + \frac{1}{2}E_{\text{O}_2} - E_{\text{surface}}$$

The hydrogen absorption energy (E_{Hads}) was calculated with the equation $E_{\text{Hads}} = E_{\text{surface+H}} - (E_{\text{surface}} + E_{\text{H}})$. The energies of E_{O_2} and E_{H} were computed by placing the adsorbate in a cubic cell with a 15 Å wide vacuum in each direction. Transition states (TS) were determined with the dimer method⁴¹ and the climbing-image nudged elastic band method⁴² with a force convergence of 0.05 eV Å⁻¹.

3. Results and discussion

3.1 Descriptors of oxygen reactivity

The cubic perovskite (001) surface can have both the ‘A’ and ‘B’ terminations (Fig. 1). On each model termination, there is one possible lattice oxygen site for catalysis. On the ‘A’ surface, the oxygen is fourfold-coordinated to the surface A cation and onefold-coordinated to the subsurface B cation. On the ‘B’ surface, the oxygen is twofold-coordinated to the surface B cation and twofold-coordinated to the subsurface A cation. We are interested in these oxygen sites’ activity for alkane activation. The first C–H bond breaking is regarded to be rate limiting in many cases of alkane activation;^{25,26} therefore, the C–H activation energy can be a useful quantity to predict the overall ability of a surface to react with methane. Furthermore, conclusions regarding the relative reactivity for methane activation can be applied to other similar C–H activation energies for other alkanes.¹³ On metal oxides, the reactive lattice oxygen activates the molecule *via* homolytic cleavage of the C–H bond (illustrated in Fig. 1a), and the perovskite (001) surfaces follow the same mechanism. H adsorption energy (HAE) and O vacancy formation energy (OVFE) are the commonly used energy descriptors for oxygen reactivity, so we explored their correlation with the C–H activation energy for the A- and B-terminations of many cubic ABO₃ perovskites. Fig. 2 shows the correlation between HAE and C–H E_{a} ($R = 0.99$, MAE = 0.10 eV) and between OVFE and C–H E_{a} ($R = 0.97$, MAE = 0.19 eV). Example geometries for the C–H activation transition states can be found in Fig. 1b. The good linear correlations suggest that one can use either HAE or OVFE as a descriptor to predict E_{a} : the stronger the H adsorption on the lattice oxygen or the easier the formation of an oxygen vacancy at the lattice-oxygen site, the lower the C–H activation energy of methane.

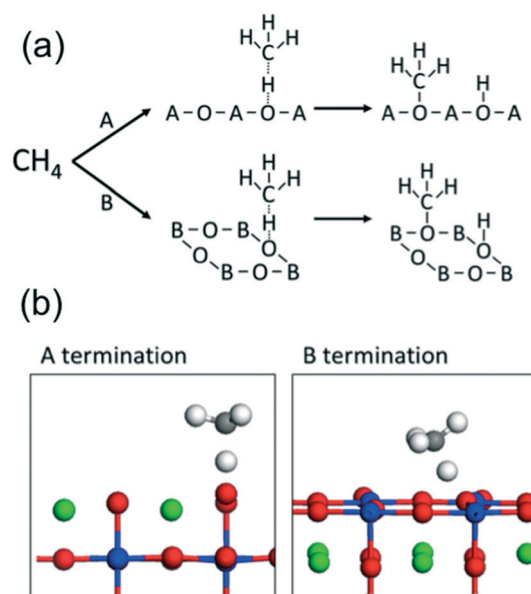


Fig. 1 CH₄ activation on the perovskite (001) A and B terminations: (a) the homolytic C–H pathway; (b) typical transition states (A atom, green; B atom, blue; O, red; C, grey; H, white).

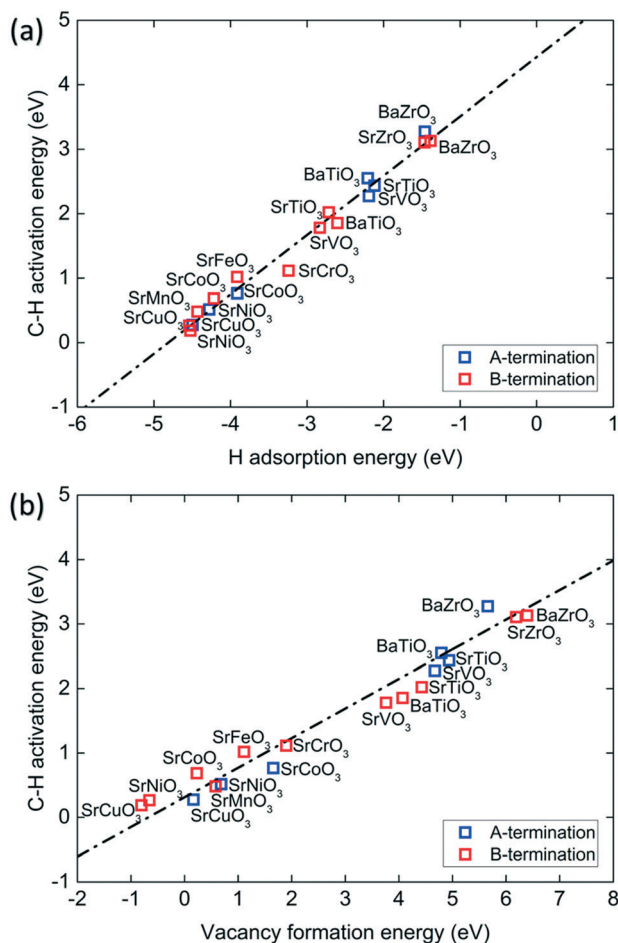


Fig. 2 Correlation between homolytic C-H activation energy of CH₄ and hydrogen adsorption energy (a) and oxygen vacancy formation energy (b). The lines represent the best linear fit.

The activity of the lattice oxygen can also play an additional role beyond the direct activation of the C-H such as oxygen transport and recombination.^{43,44} In particular, the existing descriptor OVFE could possibly relate to the activity of oxygen for these processes. OVFE directly correlates with the thermodynamic barrier for the removal of oxygen lattice and, by extension, the strength of the M-O bond. Furthermore, the formation of vacancies can have an important role in controlling the rate of oxygen activation on the surface.⁴⁵ Unsurprisingly, as both HAE and OVFE relate well to C-H activation, we can find a strong linear correlation between HAE and OVFE as shown in Fig. 3. Therefore, we can reduce the ability to activate C-H and form oxygen vacancies on the surface to a single parameter. Below we analyze in detail the trend of the oxygen reactivity from the perspectives of A cations, B cations, and their terminations.

3.2 Impact of the A cation on oxygen reactivity

Fig. 4 shows that changing the identity of the A cation within the same group (Ca to Sr) has a negligible impact (~ 0.1 eV) on HAE. This is true regardless of the termination of the sur-

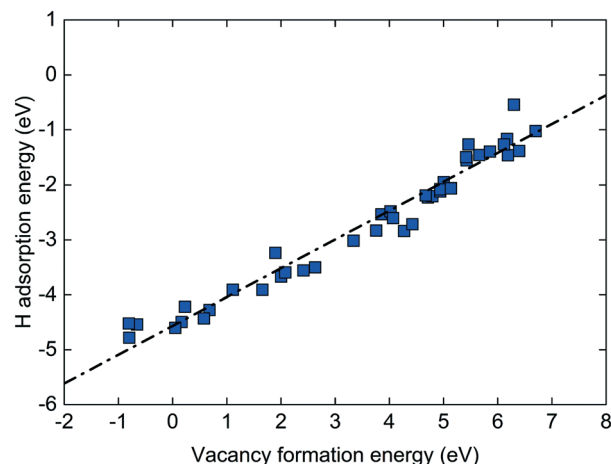


Fig. 3 Correlation between hydrogen adsorption energy and vacancy formation energy of the lattice oxygen. The black line represents the best linear fit.

face. For comparison, the HAE on the pure alkali earth oxides varies by about 0.8 eV among CaO, BaO, and SrO. In other words, even though the A termination exposes only the alkali earth metal and O ions, the reactivity of oxygen is still dictated by the underlying B transition metal. Another common A cation in perovskites is lanthanum⁶ which has a charge of +3 instead of +2. Correspondingly, the oxidation state of the B cation becomes +3 instead of +4, which has a significant impact on the bonding with oxygen. This results in both strengthening of the B-O bond and diminishing the reducibility of the B atom, leading to a lower HAE (Fig. 4). Therefore, selecting a suitable A cation should be driven by oxidation states rather than by the size of the ions, provided that they are sufficient to form a stable perovskite.

3.3 Impact of the B cation on oxygen reactivity

Fig. 5a shows that within one period, the difference in HAE between SrTiO₃ and SrCuO₃ is over 2 eV for the A termination and about 1.5 eV for the B termination. In other words, the oxygen reactivity on both terminations increases from Ti to Cu. One can understand this trend from the B-O bond strength across the period: as the number of d-electrons increases along the same period, weakening of the B-O bond occurs due to the filling of the anti-bonding orbitals, leading to higher oxygen reactivity. Fig. 5c and d shows that within a group, the HAE decreases or the oxygen reactivity decreases going down the periodic table, such as from Ti to Zr to Hf, which corresponds to decreasing electronegativity or increasing metallicity from Ti (1.54) to Zr (1.33) and Hf (1.30). In other words, oxygen becomes more ionic and less reactive toward atomic hydrogen.

The strong influence of the B cation compared to the A cation on HAE and hence oxygen reactivity demonstrates the primary role of the transition metal B cations in controlling perovskite reducibility. On reducible metal oxides, the formation of a vacancy or the adsorption of hydrogen results in the

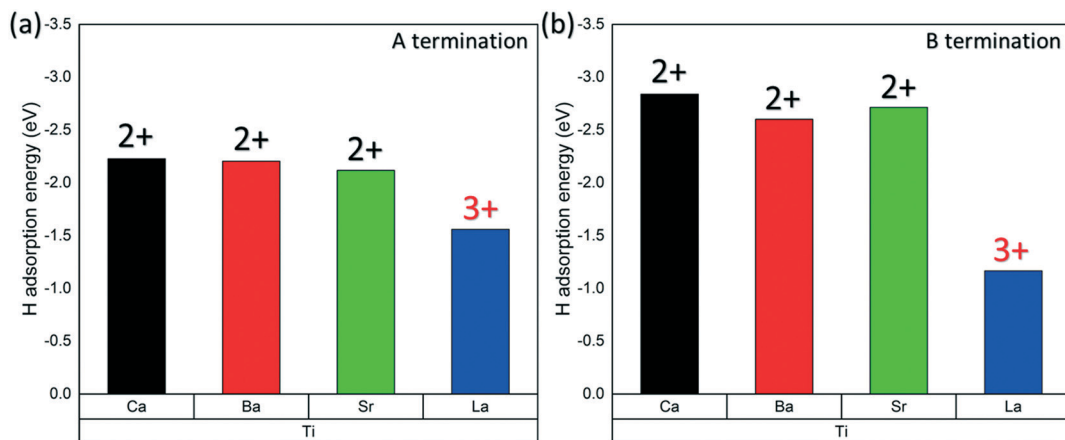


Fig. 4 Hydrogen adsorption energy for perovskites with different A cations: (a) A termination; (b) B termination. The numbers at the top of the bars show the oxidation states of the A cations.

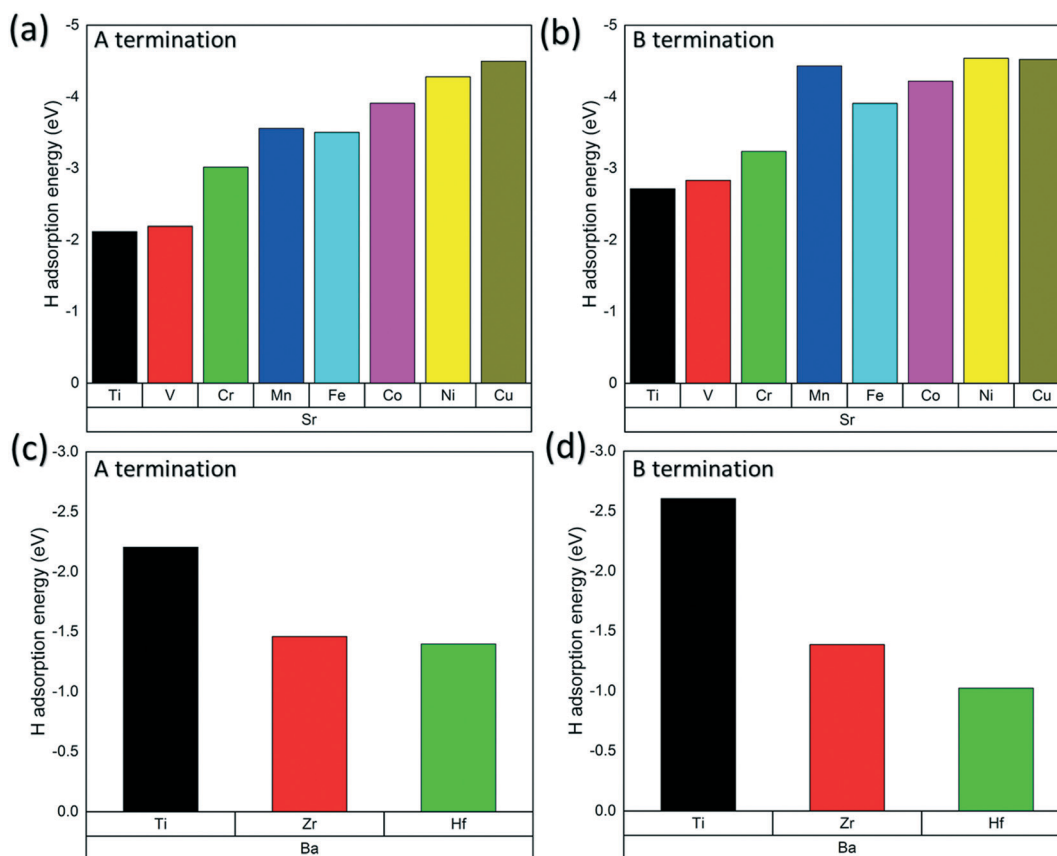


Fig. 5 Hydrogen adsorption energy for perovskites with different B cations: (a) across a period for the A termination; (b) across a period for the B termination; (c) down the same group for the A termination; (d) down the same group for the B termination.

donation of electrons to the neighboring metal.^{15,17} For comparatively irreducible oxides such as alkali earth oxides, the electron(s) is instead delocalized over the system.¹⁴ In the perovskite, the extra electrons will reduce the B cation much like in the cases of reducible metal oxides. Meanwhile, the A cations (with the same oxidation state) will have very little

impact on the reducibility of the surface as the electron will not become delocalized like in the pure alkali metal oxide. Furthermore, the O–B bond distance is always shorter than the O–A bond distance,⁴⁶ which provides a much more viable channel for electron transfer. This can explain why changing the A cation from Ca to Sr to Ba has very little impact on the

surface reducibility, while changing the B cation has a much greater effect.

3.4 Impact of termination on oxygen reactivity

To compare the two terminations of the same facet, we plotted the difference in HAE between A and B terminations. Fig. 6 shows that for most of the perovskites examined, the B termination is more active. The reason can be traced to the different coordination environment of the lattice oxygen atoms. The oxygen is doubly coordinated to the B cation on the B termination but only singly coordinated on the A termination. Given that the nearby B cations are reduction centers, the presence of an additional O–B coordination can aid the reducibility of the oxygen. This is also consistent with our finding that the reducibility of the surface is primarily directed by the B cation. In particular, ASnO_3 , ATiO_3 , AVO_3 and AMnO_3 show significant differences in oxygen reactivity on the two terminations, with the largest difference being on the order of over 1 eV for ASnO_3 . A difference of this magnitude suggests that experimentally altering the termination can provide another dimension for controlling catalyst activity. For LaTiO_3 , BaZrO_3 and BaHfO_3 , the oxygen on the A termination is more reactive. In the case of LaTiO_3 , the more reducible La (A-termination) replaces Ti (B-termination) as the reduction center on the surface. Similarly, ZrO_2 and HfO_2 are highly irreducible oxides⁴⁷ and even more irreducible than the alkali earth metals, resulting in less reducible B termination surfaces as well.

3.5 Second C–H activation or oxidative coupling on perovskites

Further oxidation of adsorbed methyl to the CO_x products proceeds *via* the further cleavage of C–H bonds. We examined the cleavage of $\text{H-CH}_2\text{O}^*$, as this step is generally irreversible and will proceed down to CO_x . Fig. 7 shows the transition states for $\text{H-CH}_2\text{O}^*$ cleavage. The $\text{CH}_4 \rightarrow \text{CH}_3$ transition state (Fig. 1b) involves only the oxygen site, whereas the $\text{H-CH}_2\text{O}^* \rightarrow \text{H}^* + \text{CH}_2\text{-O}^*$ transition state shows

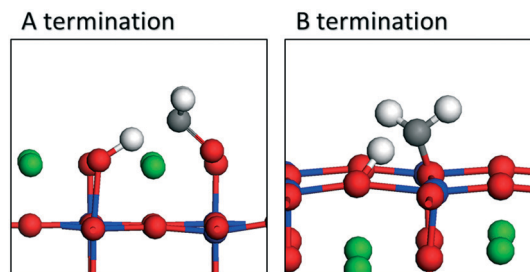


Fig. 7 Typical transition states for the 2nd C–H activation of methane ($\text{H-CH}_2\text{O}^* \rightarrow \text{H}^* + \text{CH}_2\text{-O}^*$) on A termination and B termination of a perovskite (001) surface.

close proximity of the adsorbate species with the metal cations. Unlike the highly linear correlation between the 1st C–H activation and HAE (Fig. 2a), the correlation between the 2nd C–H activation and HAE (Fig. 8) shows large deviations from the trend line. First, some perovskites and facets have higher than expected 2nd C–H activation energies, such as the A termination of BaBO_3 ($\text{B} = \text{Ti}, \text{Zr}, \text{and Hf}$) and non-transition metal B cations such as ASnO_3 ($\text{A} = \text{Sr}, \text{Ba}$). The large Ba cation will sterically hinder the C–H activation of the methoxide to the nearby oxygen, which straddles between two Ba cations on the A termination. The Sn cation performs worse than the transition metal B cations in stabilizing the methoxide C–H activation on the B termination.

Instead of the second C–H activation, the CH_3 groups can desorb from the surface oxygen site and couple in the gas phase to form C_2 products.²⁵ Interestingly, we found that CH_3 desorption energy also linearly correlates with hydrogen adsorption energy (HAE) for both A and B terminations, as seen in Fig. 9. This means that the termination sensitivity found in Fig. 6 (as reflected in the difference in HAE between A and B terminations) also applies to CH_3 desorption energy. Fig. 9 shows that very negative HAE correlates to very positive CH_3 desorption energy. In other words, while stronger H adsorption leads to easier first C–H activation, it also causes more difficult methyl desorption. As a result, the perovskites at the intersection between the two scaling lines offer a good

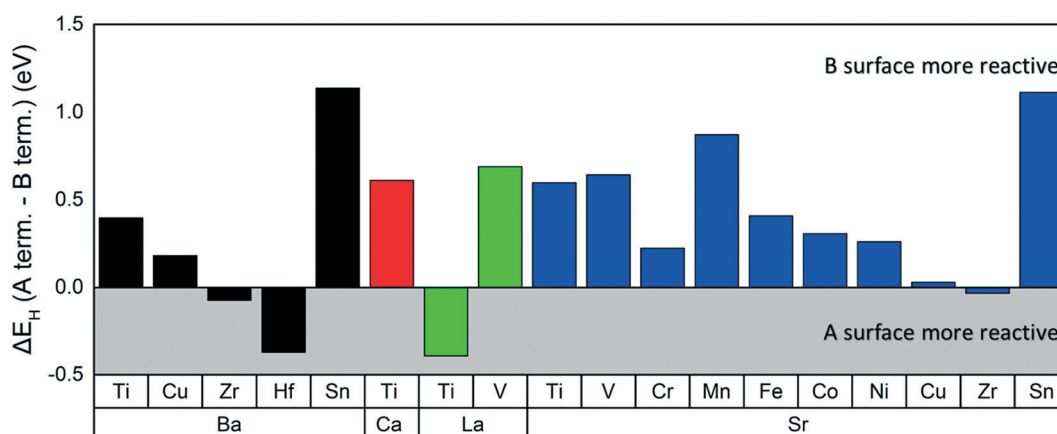


Fig. 6 Difference in hydrogen adsorption energy between the A and B terminations of the (001) facet.

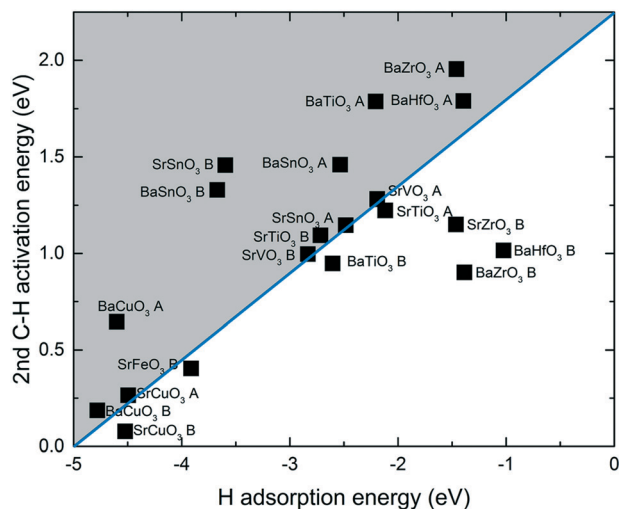


Fig. 8 Correlation between 2nd C–H activation energy of methane ($\text{H}-\text{CH}_2\text{O}^* \rightarrow \text{H}^* + \text{CH}_2-\text{O}^*$) and H adsorption energy. The blue line is a visual aid for the linear correlation between the two quantities.

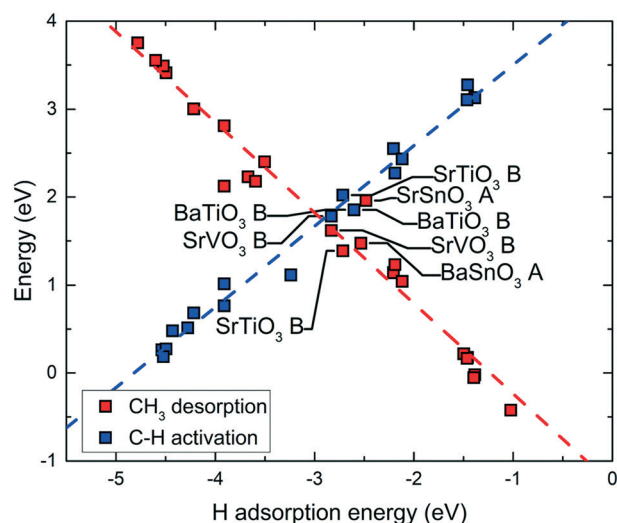


Fig. 9 Correlation between CH_3 desorption energy (red) with hydrogen adsorption energy. For comparison, correlation between C–H activation energy (blue) with hydrogen adsorption energy is also shown. The dashed lines represent the best linear fits.

balance between first C–H activation and methyl desorption, which is more conducive towards the coupling products.

3.6 Implications

Due to the diversity of possible perovskite compositions, it is imperative to obtain useful design principles in order to identify the most promising perovskite compositions for targeted experimental preparation and characterization. The descriptor-based approach is useful in quickly obtaining general and reliable catalyst properties from first principles. Descriptors for metal oxides have only recently begun gaining general attention,¹³ given the inherent electronic and structural complexity of the system compared to transition metals.

In this study, we have found hydrogen adsorption energy (HAE) to be a central descriptor for several catalytically relevant properties of the perovskites. There are several important implications from the present work. At the very negative HAE limit (namely, very strong H adsorption), C–H activation is extremely facile, but will result in low OVFE, so formation of high amounts of defects in both the surface and the bulk, especially at elevated temperatures, can have a detrimental effect on the catalytic activity by reducing the fraction of available active sites¹³ and affecting the structural stability. Very negative HAE also leads to difficult CH_3 desorption which is detrimental to the formation of C_2 products in the gas phase. At the limit of very weak H adsorption, C–H activation becomes difficult, but the catalyst surface is expected to be more stable and desorption of the methyl groups is favorable. These observations suggest the Sabatier principle^{10,48,49} at work: surfaces which are neither too reactive nor too inert (too high or too low hydrogen adsorption) offer the optimal performance.

It is desirable to compare our prediction here with previous experimental studies of perovskites for methane activation. We predict that perovskites with $\text{B} = \text{Mn}$ to Cu are the most active for homolytic C–H activation, which is supported by some experimental results.^{2,3,5,50,51} On the other hand, we predict perovskites with B in group 5 or lower (such as Ti , Zr , Hf) to be less active for C–H activation, though experimental results show that catalysts such as SrTiO_3 are still active for methane combustion.^{52,53} One explanation is that in our model we considered only the (001) surface with perfect A or B termination (instead of other facets and mixed terminations). In addition, we only examined the initial steps of methane activation instead of the whole catalytic pathway. Further work is warranted to improve our modeling. Nevertheless, we have demonstrated that HAE can be a valuable litmus test of perovskite activity in its various linear scaling relationships.

4. Conclusions

We have correlated oxygen reactivity descriptors such as oxygen vacancy formation energy and hydrogen adsorption energy with methane C–H activation energy among a large set of perovskite compositions. For the same B cation, changing the A cation within the same group has a negligible effect on oxygen reactivity, but the effect becomes significant when changing between different oxidation states for A such as from Sr^{2+} to La^{3+} . Meanwhile, the reducibility and, by extension, the redox reactivity of the lattice oxygen is largely driven by the B cation, and can vary significantly within a period; perovskites with late transition metals have the most reactive oxygen. For the same reason, the activity of the B termination is higher than the A termination in most cases. To select perovskites for high 2nd C–H activation energies to avoid combustion to CO and CO_2 , we found that larger A cations and non-transition metal B cations (with BaSnO_3 as a promising example) may lead to higher selectivity and yields for C_2

products. The tradeoff between the first C–H bond breaking and methyl desorption suggests a sweet-spot of oxygen reactivity for oxidative methane coupling. This study presents an initial attempt toward addressing the compositional diversity of perovskites in the context of energetic descriptors for methane activation.

Conflicts of interest

There are no conflicts of interest to declare.

Acknowledgements

This research is sponsored by the U.S. Department of Energy, Office of Science, Office of Basic Energy Sciences, Chemical Sciences, Geosciences, and Biosciences Division. This research used resources of the National Energy Research Scientific Computing Center, a DOE Office of Science User Facility supported by the Office of Science of the U.S. Department of Energy under Contract No. DE-AC02-05CH11231.

References

- V. M. Goldschmidt, *Naturwissenschaften*, 1926, **14**, 477–485.
- H. Arai, T. Yamada, K. Eguchi and T. Seiyama, *Appl. Catal.*, 1986, **26**, 265–276.
- M. Pena and J. Fierro, *Chem. Rev.*, 2001, **101**, 1981–2018.
- J. Zhu, H. Li, L. Zhong, P. Xiao, X. Xu, X. Yang, Z. Zhao and J. Li, *ACS Catal.*, 2014, **4**, 2917–2940.
- S. Royer, D. Duprez, F. Can, X. Courtois, C. Batiot-Dupeyrat, S. Laassiri and H. Alamdari, *Chem. Rev.*, 2014, **114**, 10292–10368.
- H. Zhu, P. Zhang and S. Dai, *ACS Catal.*, 2015, **5**, 6370–6385.
- N. Labhasetwar, G. Saravanan, S. K. Megarajan, N. Manwar, R. Khobragade, P. Doggali and F. Grasset, *Sci. Technol. Adv. Mater.*, 2015, **16**, 036002.
- W. Wang, M. O. Tadé and Z. Shao, *Chem. Soc. Rev.*, 2015, **44**, 5371–5408.
- J. K. Nørskov, F. Abild-Pedersen, F. Studt and T. Bligaard, *Proc. Natl. Acad. Sci. U. S. A.*, 2011, **108**, 937–943.
- J. K. Nørskov, T. Bligaard, J. Rossmeisl and C. H. Christensen, *Nat. Chem.*, 2009, **1**, 37–46.
- J. Suntivich, H. A. Gasteiger, N. Yabuuchi, H. Nakanishi, J. B. Goodenough and Y. Shao-Horn, *Nat. Chem.*, 2011, **3**, 546–550.
- G. S. Foo, F. Polo Garzon, V. Fung, D.-E. Jiang, S. H. Overbury and Z. Wu, *ACS Catal.*, 2017, **4**, 4423–4434.
- A. A. Latimer, A. R. Kulkarni, H. Aljama, J. H. Montoya, J. S. Yoo, C. Tsai, F. Abild-Pedersen, F. Studt and J. K. Nørskov, *Nat. Mater.*, 2017, **16**, 225–229.
- G. Kumar, S. L. J. Lau, M. D. Krcha and M. J. Janik, *ACS Catal.*, 2016, **6**, 1812–1821.
- M. D. Krcha, A. D. Mayernick and M. J. Janik, *J. Catal.*, 2012, **293**, 103–115.
- J. Liu, S. Zhang, Y. Zhou, V. Fung, L. Nguyen, D.-E. Jiang, W. Shen, J. Fan and F. F. Tao, *ACS Catal.*, 2016, **6**, 4218–4228.
- A. D. Mayernick and M. J. Janik, *J. Phys. Chem. C*, 2008, **112**, 14955–14964.
- B. Beck, M. Harth, N. G. Hamilton, C. Carrero, J. J. Uhlrich, A. Trunschke, S. Shaikhutdinov, H. Schubert, H.-J. Freund and R. Schlögl, *J. Catal.*, 2012, **296**, 120–131.
- A. R. Derk, B. Li, S. Sharma, G. M. Moore, E. W. McFarland and H. Metiu, *Catal. Lett.*, 2013, **143**, 406–410.
- P. Schwach, X. Pan and X. Bao, *Chem. Rev.*, 2017, **117**, 8497–8520.
- Y. Amenomiya, V. I. Birss, M. Goledzinowski, J. Galuszka and A. R. Sanger, *Catal. Rev.: Sci. Eng.*, 1990, **32**, 163–227.
- T. Choudhary, S. Banerjee and V. Choudhary, *Appl. Catal., A*, 2002, **234**, 1–23.
- D. Pakhare and J. Spivey, *Chem. Soc. Rev.*, 2014, **43**, 7813–7837.
- J. Chen, H. Arandiyana, X. Gao and J. Li, *Catal. Surv. Asia*, 2015, **19**, 140–171.
- J. H. Lunsford, *Angew. Chem., Int. Ed. Engl.*, 1995, **34**, 970–980.
- H. Schwarz, *Angew. Chem., Int. Ed.*, 2011, **50**, 10096–10115.
- R. Horn and R. Schlögl, *Catal. Lett.*, 2015, **145**, 23–39.
- C. Coperet, *Chem. Rev.*, 2009, **110**, 656–680.
- E. C. Tyo, C. Yin, M. Di Vece, Q. Qian, G. Kwon, S. Lee, B. Lee, J. E. DeBartolo, S. Seifert, R. E. Winans, R. Si, B. Ricks, S. Goergen, M. Rutter, B. Zugic, M. Flytzani-Stephanopoulos, Z. W. Wang, R. E. Palmer, M. Neurock and S. Vajda, *ACS Catal.*, 2012, **2**, 2409–2423.
- V. Fung, F. F. Tao and D.-E. Jiang, *Catal. Sci. Technol.*, 2016, **6**, 6861–6869.
- H. Zheng, Q. Zhan, F. Zavaliche, M. Sherburne, F. Straub, M. P. Cruz, L.-Q. Chen, U. Dahmen and R. Ramesh, *Nano Lett.*, 2006, **6**, 1401–1407.
- H. Tanaka, H. Tabata and T. Kawai, *Thin Solid Films*, 1999, **342**, 4–7.
- N. Erdman, K. R. Poeppelmeier, M. Asta, O. Warschkow, D. E. Ellis and L. D. Marks, *Nature*, 2002, **419**, 55–58.
- F. Polo-Garzon, S.-Z. Yang, V. Fung, G. S. Foo, E. E. Bickel, M. F. Chisholm, D.-E. Jiang and Z. Wu, *Angew. Chem., Int. Ed.*, 2017, **56**, 9820–9824.
- G. Kresse and J. Furthmüller, *Comput. Mater. Sci.*, 1996, **6**, 15–50.
- G. Kresse and J. Furthmüller, *Phys. Rev. B: Condens. Matter Mater. Phys.*, 1996, **54**, 11169–11186.
- J. P. Perdew, K. Burke and M. Ernzerhof, *Phys. Rev. Lett.*, 1996, **77**, 3865.
- P. E. Blöchl, *Phys. Rev. B: Condens. Matter Mater. Phys.*, 1994, **50**, 17953–17979.
- H. J. Monkhorst and J. D. Pack, *Phys. Rev. B: Solid State*, 1976, **13**, 5188.
- S. Grimme, J. Antony, S. Ehrlich and H. Krieg, *J. Chem. Phys.*, 2010, **132**, 154104.
- G. Henkelman and H. Jónsson, *J. Chem. Phys.*, 1999, **111**, 7010.
- G. Henkelman, B. P. Uberuaga and H. Jónsson, *J. Chem. Phys.*, 2000, **113**, 9901–9904.
- I. Rossetti, M. Allieta, C. Biffi and M. Scavini, *Phys. Chem. Chem. Phys.*, 2013, **15**, 16779–16787.

- 44 I. Rossetti, C. Biffi and L. Forni, *Chem. Eng. J.*, 2010, **162**, 768–775.
- 45 A. Staykov, H. Téllez, T. Akbay, J. Druce, T. Ishihara and J. Kilner, *Chem. Mater.*, 2015, **27**, 8273–8281.
- 46 Z. Zeng, F. Calle-Vallejo, M. B. Mogensen and J. Rossmeisl, *Phys. Chem. Chem. Phys.*, 2013, **15**, 7526–7533.
- 47 F. McTaggart, *Nature*, 1961, **191**, 1192–1192.
- 48 A. J. Medford, A. Vojvodic, J. S. Hummelshøj, J. Voss, F. Abild-Pedersen, F. Studt, T. Bligaard, A. Nilsson and J. K. Nørskov, *J. Catal.*, 2015, **328**, 36–42.
- 49 P. Sabatier, *Eur. J. Inorg. Chem.*, 1911, **44**, 1984–2001.
- 50 J. Tascon and L. G. Tejuca, *React. Kinet. Catal. Lett.*, 1980, **15**, 185–191.
- 51 R. J. Voorhoeve, J. Remeika, P. Freeland and B. Matthias, *Science*, 1972, **177**, 353–354.
- 52 C. Oliva, S. Cappelli, I. Rossetti, A. Kryukov, L. Bonoldi and L. Forni, *J. Mol. Catal. A: Chem.*, 2006, **245**, 55–61.
- 53 C. Oliva, L. Bonoldi, S. Cappelli, L. Fabbrini, I. Rossetti and L. Forni, *J. Mol. Catal. A: Chem.*, 2005, **226**, 33–40.